Topological Transition of Superconductivity in Dirac Semimetal Nanowire Josephson Junctions

Cai-Zhen Li,[1,2,*] An-Qi Wang,[2,3,*] Chuan Li,[4,†] Wen-Zhuang Zheng,[2] Alexander Brinkman,[4] Da-Peng Yu,[1] and Zhi-Min Liao[2,5,‡]

[1]*Shenzhen Institute for Quantum Science and Engineering, and Department of Physics, Southern University of Science and Technology, Shenzhen 518055, China*

[2]*State Key Laboratory for Mesoscopic Physics and Frontiers Science Center for Nano-optoelectronics, School of Physics, Peking University, Beijing 100871, China*

[3]*Academy for Advanced Interdisciplinary Studies, Peking University, Beijing 100871, China*

[4]*MESA+ Institute for Nanotechnology, University of Twente, 7500 AE Enschede, The Netherlands*

[5]*Beijing Key Laboratory of Quantum Devices, Peking University, Beijing 100871, China*

(Received 20 October 2020; accepted 18 December 2020; published 12 January 2021)

We report the topological transition by gate control in a Cd_3As_2 Dirac semimetal nanowire Josephson junction with diameter of about 64 nm. In the electron branch, the quantum confinement effect enforces the surface band into a series of gapped subbands and thus nontopological states. In the hole branch, however, because the hole mean free path is smaller than the nanowire perimeter, the quantum confinement effect is inoperative and the topological property maintained. The superconductivity is enhanced by gate tuning from electron to hole conduction, manifested by a larger critical supercurrent and a larger critical magnetic field, which is attributed to the topological transition from gapped surface subbands to a gapless surface band. The gate-controlled topological transition of superconductivity should be valuable for manipulation of Majorana zero modes, providing a platform for future compatible and scalable design of topological qubits.

DOI: 10.1103/PhysRevLett.126.027001

Much effort has been paid to find routes for the realization of topological superconductivity in several platforms, ranging from the presumably intrinsic topological superconductors [1–3], topological materials [4], and semiconductor nanowires [5,6] proximitized with an *s*-wave superconductor, ferromagnetic atomic chains [7,8], and iron-based superconductors [9–12], etc. The topological superconducting phase transition has been obtained by applying a magnetic field in semiconductor nanowires coupled with a superconductor, showing the signatures of Majorana fermions [13–15]. Recently, topological transitions have also been proposed based on Josephson junctions in a 2D electron gas [16–19], which can be tuned by a superconducting phase difference. In addition, the topological superconductivity can be realized in the topological surface and edge states proximitized with a superconductor [4,20–28].

The topological transition of topological materials themselves will trigger the phase transition of the proximity-induced topological superconductivity accordingly. Such a topological phase transition can be realized by magnetic-field-induced opening and closing of the Dirac gap [29,30], electric-field control [31–33], applying strain or high pressure [34–38], etc. In addition, the quantum confinement also provides a way to induce discrete surface subbands in thin nanowires. Tuning the quantum confinement will tune the phase transition with opening and closing of the surface Dirac gap, accompanied by the presence or absence of quantized surface subbands. Combining the topological transition with superconductivity opens an avenue for fine control of Majorana zero modes.

Here we report the topological transition of superconductivity in Cd_3As_2 Dirac semimetal nanowire-based Josephson junctions by gate control [Fig. 1(a)]. The Cd_3As_2 nanowires were grown by chemical vapor deposition method [39], which are of single crystalline nature and grown along the [110] direction (see Supplemental Material, Fig. S1 [40]). The topological transition of Cd_3As_2 surface states is revealed by quantum oscillations under a magnetic field parallel to the nanowire axis. Because of the relatively high electron mobility and low hole mobility in Cd_3As_2 [43–45], the quantum confinement effect could be notable for the electron conduction and negligible for hole conduction in a thin nanowire with diameter of ~64 nm in this Letter [Fig. 1(b)]. Because the mean free path of electrons is comparable with the nanowire perimeter, Aharonov-Bohm (AB) oscillations with flux quantum (h/e) periodicity are expected [46,47]. Whereas, for the diffusive transport of holes, the Altshuler-Aronov-Spivak (AAS) oscillations with $h/2e$ period become prominent. A clear transition from h/e period AB oscillations ($\Delta B = 1.28$ T) to $h/2e$ period AAS

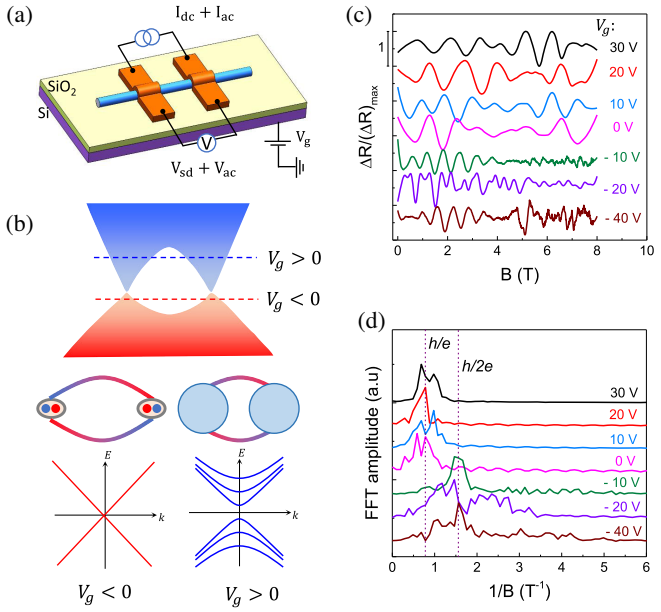

FIG. 1. Normal state transport in Nb-Cd_3As_2-Nb junction. (a) Schematic of the measurement setup. The junction length is ~400 nm. (b) Top: the bulk bands schematic diagram of Cd_3As_2. Middle: the schematic of Fermi arc surface states. Bottom: the continuous Dirac surface band for $V_g < 0$ and quantized surface subbands due to quantum confinement effect for $V_g > 0$. (c) The normalized resistance oscillations $\Delta R/(\Delta R)_{max}$ after subtracting the background. The magnetic field is applied in plane along the nanowire axis. (d) FFT spectrums of the resistance oscillations under different gate voltages.

oscillations ($\Delta B = 0.64$ T) is observed by tuning the gate voltage from positive to negative [Figs. 1(c) and 1(d); the raw data in Fig. S2 [40]], indicating a transition from gapped quantized surface subbands to a gapless surface band.

We then focus on the superconducting behavior with and without the quantized surface subbands at a base temperature of 12 mK. Figure 2(a) shows the current-voltage (I_{dc}-V_{sd}) characteristics of the junction. The superconducting state shows a critical current I_c varying with V_g. The differential resistance dV/dI as a function of V_g and I_{dc} is presented in Fig. 2(b), and the I_c is marked by the solid white line. As sweeping V_g from 18 to −30 V, the I_c decreases first and then tends to saturate in the hole region. The small and saturated I_c in the hole region is due to the low hole mobility, where the supercurrent through bulk states is significantly suppressed [25,48]. An excess current I_{exc} ~210 nA in the I-V characteristic gives a transparency $D \sim 0.73$ of the junction interface [49] (Supplemental Material, Fig. S3 [40]).

An in-plane magnetic field B is applied along the nanowire axis. Figure 2(c) shows the dV/dI as a function of B and I_{dc} at $V_g = 0$ V. From 0 to 250 mT, I_c is strongly suppressed from 180 to 3 nA. Beyond the initial fast decay, the $I_c(B)$ exhibits an irregular oscillation behavior with multiple nodes, which can be seen up to 2 T. Figures 2(d)–2(f) show the enlarged $I_c(B)$ oscillations at three different gate voltages. The $I_c(B)$ exhibits multiple nodes at $V_g = 22$ and 0 V [Figs. 2(d) and 2(e)], while only two nodes at $V_g = -30$ V [Fig. 2(f)]. The successive evolution of $I_c(B)$ oscillations as a function of V_g is displayed in Fig. 2(g). For positive V_g, the $I_c(B)$ shows multiple nodes with maxima and minima sensitively depending on V_g. For negative V_g, only two nodes are observed and the period is gate independent. Note that the $I_c(B)$ oscillatory behavior can only be observed when the magnetic field is applied along the nanowire axis. While under an in-plane magnetic field perpendicular to the nanowire axis, the $I_c(B)$ exhibits a monotonic decay without any oscillations (Supplemental Material, Fig. S4 [40]).

This distinct gate dependence of the $I_c(B)$ oscillatory behavior can be well explained by considering the presence (absence) of quantized surface subbands at positive (negative) V_g. For positive V_g at zero magnetic field, it is natural that the supercurrent is from the coexisting bulk and surface states due to the highly conductive bulk and large surface-to-volume ratio in Cd_3As_2 nanowires. When applying a magnetic field, the bulk carried supercurrent is strongly suppressed (as indicated by the I_c kink behavior at around 0.15 T in Fig. 2(i); also see Supplemental Material, Figs. S5 and S6 [40]), while the supercurrent carried by surface states can survive to high magnetic fields [50]. So, the I_c oscillations under high magnetic fields should be attributed to the quantized surface subbands.

Below, we illustrate how the quantized surface subbands result in I_c oscillations. The quantized surface subbands can be described by the angular momentum quantum number l [30,47]. In the presence of a parallel magnetic field, the motion of particles on the nanowire surface travels in a spiraled path when they traverse the junction from one Nb electrode to the other [Fig. 2(h)]. Different surface modes with different quantized angular momentum l traverse a different path along the nanowire and thus acquire a different orbital phase $\Delta\phi = (2e/\hbar)\int_{\theta_1}^{\theta_2} \vec{A} \cdot R d\theta_l$, where $\vec{A}$ is the vector potential, R is the radius, and θ_l is the corresponding winding angle. The quantum interference between supercurrents carried by different surface modes consequently leads to the multiple I_c oscillation nodes [51–53]. Since the occupation of surface modes can be modulated by a gate voltage, the oscillation nodes are gate sensitive. The red line in Fig. 2(d) is the numerical simulation of supercurrent interference with occupied surface modes $|l| \leq 8$ (see Supplemental Material, Figs. S5 and S6 [40] for more details). The occupied multiple orbital modes with $|l| \leq 8$ at $V_g = 22$ V are roughly consistent with the allowed number of modes in the surface states. For a carrier density n_c of the order of 10^{18} cm^{-3}, the corresponding Fermi wave

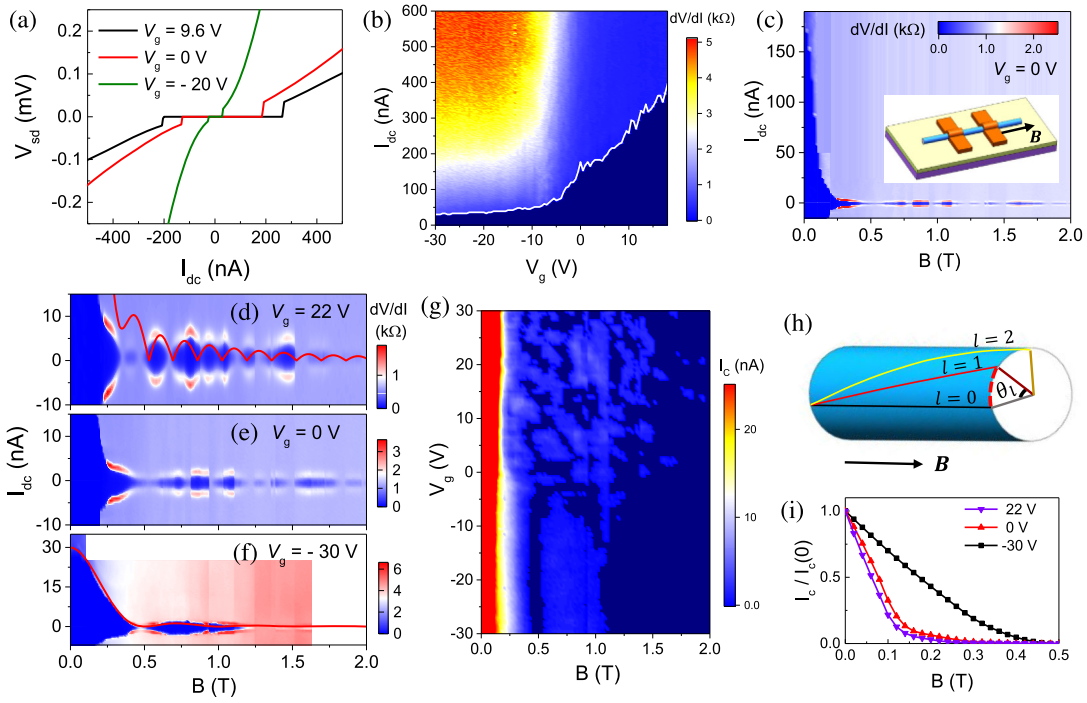

FIG. 2. The supercurrent and I_c evolution with the axial magnetic field. (a) The V_{sd} versus I_{dc} characteristics. (b) Differential resistance dV/dI as a function of I_{dc} and V_g. An excitation of $I_{ac} = 0.5$ nA was used for the dV/dI measurement. The solid white line marks the critical current I_c varying with V_g. (c) Mapping of dV/dI as a function of I_{dc} and magnetic field at $V_g = 0$ V. The I_{dc} is swept from negative to positive. Inset: schematic of the Nb-Cd_3As_2-Nb junction with an in-plane magnetic field along the nanowire direction. (d)–(f) The detailed patterns of dV/dI as a function of I_{dc} and magnetic field at different V_g. Red curve in (d): the I_c fit by the model of supercurrent interference between different surface modes. Red curve in (f): the I_c fit by the model of continuous surface band, with both orbital and Zeeman phase modulation considered. (g) Mapping of critical current I_c as a function of V_g and magnetic field. (h) Schematic of the supercurrent interference between different surface modes characterized by the angular momentum quantum number l. θ_l is the corresponding winding angle. (i) The normalized critical current $I_c/I_c(0)$ as a function of magnetic field.

vector is $k_f \sim 3\times10^8$ m^{-1}. Considering that $k_\theta = (1/R) = 3\times10^7$ m^{-1}, the maximum value of quantum number l is about $(k_f/k_\theta) \sim 10$. Therefore, most of the circular modes contribute to the supercurrent. For $V_g = 0$ V, the I_c values are very small and cannot be simulated properly, and the oscillation behavior is likely disturbed by the trapping of magnetic vortex, as indicated by the abrupt vertical lines in Fig. 2(e). The presence of vortex trapping also gives a possible origin of the slight deviation between the data and fitting curve in Fig. 2(d).

For $V_g = -30$ V, the supercurrent is mainly carried by surface states due to the low hole mobility of bulk state. With increasing magnetic field, the suppression rate of I_c at $V_g = -30$ V is much lower than that at $V_g = 22$ and 0 V [Fig. 2(i)] due to the topological protection of surface states. As a surface particle traverses along the perimeter of the nanowire from position x_1 to x_2, the phase modulation is given by $\phi_2(x_2) - \phi_1(x_1) = [\pi B(x_2 - x_1)R/\phi_0]$, where $\phi_0 = h/2e$, $\phi_1(x_1)$, and $\phi_2(x_2)$ are the phases of the order parameters (Supplemental Material, Fig. S7a [40]). As the surface bands are of continuous form without quantization at negative V_g, the integration of the supercurrent should be over the entire circle of the nanowire, which is expressed as

$$I(\varphi_0, B) \sim \int_0^{2\pi R}\int_0^{2\pi R} dx_1 dx_2 \sin[\varphi_0 + \phi_2(x_2) - \phi_1(x_1)]. \quad (1)$$

The critical current is defined as the maximum in one period of 2π phase, $I_c(B) = \max[I(\varphi_0, B)]$. As the surface particles travel through an entire circle, the period of the I_c oscillation is expected to be $\phi_0(h/2e)$, with a magnetic field period $\Delta B = 0.64$ T (Supplemental Material, Fig. S7c [40]). However, despite the fact that the normal state $h/2e$ periodic AAS oscillations demonstrate a magnetic field period of 0.64 T, the I_c oscillation in Fig. 2(f) presents a period $\Delta B = 0.5$ T. This deviation can be compensated by taking the Zeeman effect into account. When applying a magnetic field along the nanowire axis, the Fermi surface of surface state is shifted along the x direction (along the perimeter) by $(g\mu_B B/\hbar v_f)$ due to the helical spin-momentum locking property of the Fermi arc surface states [54] (Supplemental Material, Fig. S7b [40]). As a result of the shift, the Cooper pairs, formed by the electrons on the Cd_3As_2 Fermi surface, gain a finite momentum $\Delta k_x = (2g\mu_B B/\hbar v_f)$ and, consequently, acquire an extra

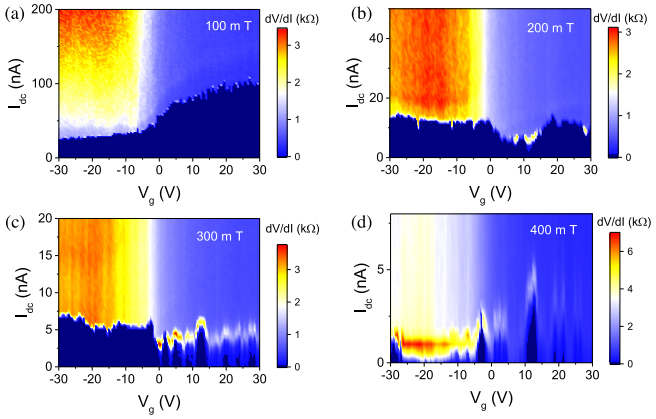

FIG. 3. (a)–(d) Mapping of dV/dI as a function of I_{dc} and V_g at different magnetic fields as denoted. At a moderate field of 300 mT, the I_c at negative V_g is larger than that at positive V_g.

phase $\Delta k_x(x_2 - x_1)$. Numerically, the experimental I_c oscillation at $V_g = -30$ V can be well fitted by summing up the orbital and Zeeman phases [red line in Fig. 2(f)]. It is necessary to note that the Zeeman effect itself could not lead to an I_c oscillation in the magnetic field range of 0–2 T (Supplemental Material, Fig. S7d [43]). The contribution of the Zeeman effect is small and it just gives a tiny modification to the period of I_c oscillation, especially in the regime of multiple surface modes at $V_g = 22$ V (Supplemental Material, Fig. S8 [40]). In addition, numerical simulations indicate that the orbital interference of bulk states only renders a monotonous I_c decay without oscillations (Supplemental Material, Fig. S9 [40]), further confirming the surface origin of I_c oscillations under higher magnetic fields.

To further study the gate control of topological phase transition, gate sweeps of the supercurrent under different magnetic fields are performed, as presented in Fig. 3. At a low field of 100 mT, because the supercurrent at positive V_g is carried by coexisting bulk and surface states, the supercurrent interference from quantized surface subbands is submerged in a large I_c background [Fig. 3(a)]. Gradually increasing the magnetic field to suppress the bulk carried supercurrent, the supercurrent interference from quantized surface subbands starts to emerge [Fig. 3(b)]. The gate control of phase transition is obtained, as the bulk carried supercurrent is fully suppressed under 300 mT [Fig. 3(c)]. In this case, with the presence of gapped surface subbands at positive V_g, the supercurrent interference between different surface modes leads to an apparent I_c oscillation behavior as tuning the occupation of surface subbands by V_g [Fig. 3(c)]. On tuning the gate voltage to negative, the low mobility of holes leads to a diffusive transport along the perimeter; thus the quantum confinement effect is inoperative and, consequently, gives rise to the preservation of gapless surface band. This is consistent with the disappearance of interference-induced I_c oscillations at negative V_g, where only a nearly flat I_c versus V_g is

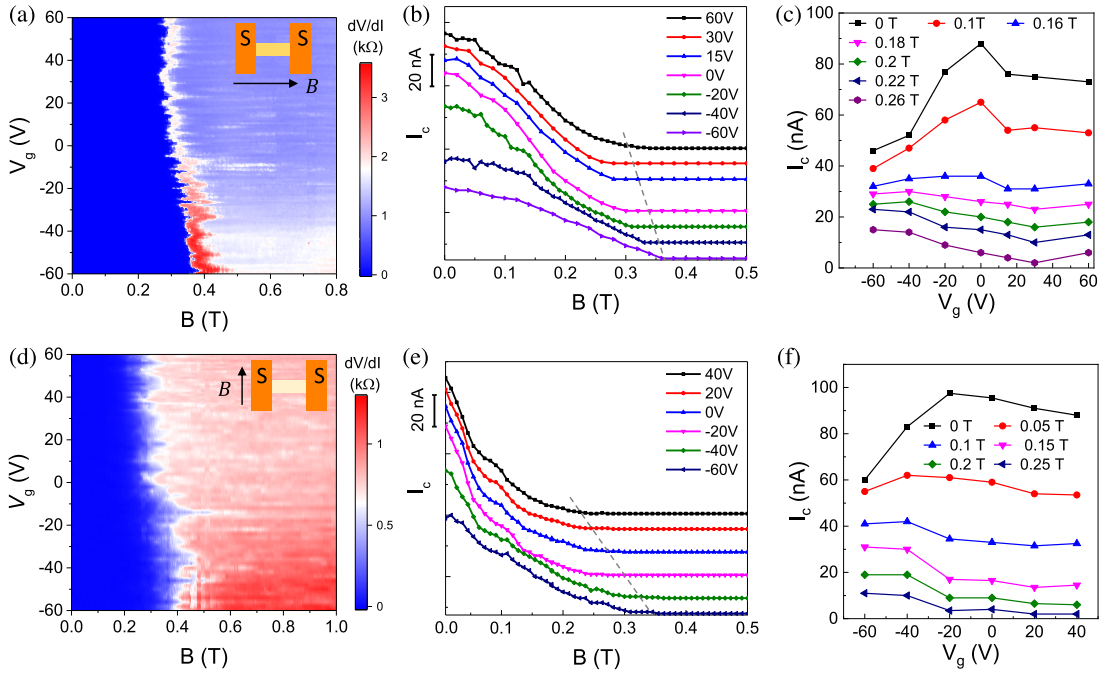

FIG. 4. The proximity-induced superconductivity in device 2 with diameter $d = 72$ nm and junction length $L = 400$ nm. (a) Color map of dV/dI as a function of magnetic field and gate voltage. Inset: the magnetic field direction with respect to the Josephson junction. S denotes superconducting electrodes. (b) The critical current I_c versus parallel magnetic field. The curves are shifted for clarity. Gray dotted line indicates the evolution of critical magnetic field B_c at which I_c decays to zero. (c) The gate dependence of I_c at different parallel magnetic fields as denoted. (d)–(f) Similar results under an in-plane perpendicular magnetic field.

observed. In addition, benefitting from the topological property of the gapless surface band, the supercurrent in this scheme is more robust than that carried by gapped surface modes, as indicated by the larger I_c amplitude at negative V_g than that at positive V_g [Fig. 3(c)].

The negative gate voltage enhanced superconductivity is also observed in a second device (device 2, with a diameter of 72 nm and junction length $L = 400$ nm). The I_c oscillations in device 2 can still be observed but are not as apparent as that in device 1 (Supplemental Material, Figs. S10 and S11 [40]), possibly due to the longer perimeter and weaker superconducting coupling. Nevertheless, it is interesting to find that the critical magnetic field B_c is enhanced as tuning the gate voltage from electron to hole conduction [Fig. 4(a)]. The enhanced B_c is also observed from the magnetic field dependence of I_c at different gate voltages, as the gray dotted line indicated in Fig. 4(b). The slower decay of I_c at negative V_g is due to the topological protection of surface states. Figure 4(c) exhibits the gate dependence of I_c at different magnetic fields. At a moderate magnetic field ($B \geq 0.18$ T), the I_c at negative V_g is larger than that at positive V_g, consistent with that shown in Fig. 3(c). Similar B_c and I_c enhancement is also observed under an in-plane perpendicular magnetic field [Figs. 4(d)–4(f)].

In summary, we have demonstrated the gate-tuned topological transition of superconductivity in Dirac semimetal nanowire Cd_3As_2 Josephson junctions. A gate-sensitive multiple-modes supercurrent interference pattern due to quantized surface subbands exists in the electron branch, and a gate-independent supercurrent oscillation in the hole branch is observed due to the gapless nature of the surface band. The critical magnetic field B_c and critical supercurrent I_c are both enhanced in the hole conduction branch, suggesting the topology enhanced superconductivity. Such gate-controlled topological transition of superconductivity is consistent with the previous observations of the presence (absence) of Majorana zero modes in the hole (electron) branch in such a similar nanowire system [25]. Our results provide a route to use Cd_3As_2 nanowire as a platform for generating and manipulating Majorana bound states, which is compatibly applicable to future networks design of braiding operations.

This work was supported by National Key Research and Development Program of China (No. 2018YFA0703703 and No. 2016YFA0300802), National Natural Science Foundation of China (No. 91964201, No. 61825401, and No. 11774004), and financially supported by Netherlands Organization for Scientific Research (NWO) through a VENI grant (680-47-463) and a VECI grant.

*C.-Z. L. and A.-Q. W. contributed equally to this work.
†chuan.li@utwente.nl
‡liaozm@pku.edu.cn

[1] T. M. Rice and M. Sigrist, Sr_2RuO_4: An electronic analogue of ^{3}He? J. Phys. Condens. Matter **7**, L643 (1995).
[2] K. Ishida, H. Mukuda, Y. Kitaoka, K. Asayama, Z. Q. Mao, Y. Mori, and Y. Maeno, Spin-triplet superconductivity in Sr_2RuO_4 identified by ^{17}O Knight shift, Nature (London) **396**, 658 (1998).
[3] G. M. Luke, Y. Fudamoto, K. M. Kojima, M. I. Larkin, J. Merrin, B. Nachumi, Y. J. Uemura, Y. Maeno, Z. Q. Mao, Y. Mori, H. Nakamura, and M. Sigrist, Time-reversal symmetry-breaking superconductivity in Sr_2RuO_4, Nature (London) **394**, 558 (1998).
[4] L. Fu and C. L. Kane, Superconducting Proximity Effect and Majorana Fermions at the Surface of a Topological Insulator, Phys. Rev. Lett. **100**, 096407 (2008).
[5] R. M. Lutchyn, J. D. Sau, and S. Das Sarma, Majorana Fermions and a Topological Phase Transition in Semiconductor-Superconductor Heterostructures, Phys. Rev. Lett. **105**, 077001 (2010).
[6] Y. Oreg, G. Refael, and F. von Oppen, Helical Liquids and Majorana Bound States in Quantum Wires, Phys. Rev. Lett. **105**, 177002 (2010).
[7] S. Nadj-Perge, I. K. Drozdov, J. Li, H. Chen, S. Jeon, J. Seo, A. H. MacDonald, B. A. Bernevig, and A. Yazdani, Observation of Majorana fermions in ferromagnetic atomic chains on a superconductor, Science **346**, 602 (2014).
[8] B. E. Feldman, M. T. Randeria, J. Li, S. Jeon, Y. Xie, Z. Wang, and I. K. Drozdov, B. Andrei Bernevig, and A. Yazdani, High-resolution studies of the Majorana atomic chain platform, Nat. Phys. **13**, 286 (2017).
[9] J. X. Yin, Z. Wu, J. H. Wang, Z. Y. Ye, J. Gong, X. Y. Hou, L. Shan, A. Li, X. J. Liang, X. X. Wu, J. Li, C. S. Ting, Z. Q. Wang, J. P. Hu, P. H. Hor, H. Ding, and S. H. Pan, Observation of a robust zero-energy bound state in iron-based superconductor Fe(Te,Se), Nat. Phys. **11**, 543 (2015).
[10] D. Wang, L. Kong, P. Fan, H. Chen, S. Zhu, W. Liu, L. Cao, Y. Sun, S. Du, J. Schneeloch, R. Zhong, G. Gu, L. Fu, H. Ding, and H.-J. Gao, Evidence for Majorana bound states in an iron-based superconductor, Science **362**, 333 (2018).
[11] P. Zhang, K. Yaji, T. Hashimoto, Y. Ota, T. Kondo, K. Okazaki, Z. Wang, J. Wen, G. D. Gu, H. Ding, and S. Shin, Observation of topological superconductivity on the surface of an iron-based superconductor, Science **360**, 182 (2018).
[12] T. Machida, Y. Sun, S. Pyon, S. Takeda, Y. Kohsaka, T. Hanaguri, T. Sasagawa, and T. Tamegai, Zero-energy vortex bound state in the superconducting topological surface state of Fe(Se,Te), Nat. Mater. **18**, 811 (2019).
[13] V. Mourik, K. Zuo, S. M. Frolov, S. R. Plissard, E. P. A. M. Bakkers, and L. P. Kouwenhoven, Signatures of Majorana fermions in hybrid superconductor-semiconductor nanowire devices, Science **336**, 1003 (2012).
[14] A. Das, Y. Ronen, Y. Most, Y. Oreg, M. Heiblum, and H. Shtrikman, Zero-bias peaks and splitting in an Al–InAs nanowire topological superconductor as a signature of Majorana fermions, Nat. Phys. **8**, 887 (2012).
[15] M. T. Deng, C. L. Yu, G. Y. Huang, M. Larsson, P. Caroff, and H. Q. Xu, Anomalous zero-bias conductance peak in a Nb-InSb nanowire-Nb hybrid device, Nano Lett. **12**, 6414 (2012).

[16] F. Pientka, A. Keselman, E. Berg, A. Yacoby, A. Stern, and B. I. Halperin, Topological Superconductivity in a Planar Josephson Junction, Phys. Rev. X **7**, 021032 (2017).
[17] A. Fornieri, A. M. Whiticar, F. Setiawan, E. Portolés, A. C. C. Drachmann, A. Keselman, S. Gronin, C. Thomas, T. Wang, R. Kallaher, G. C. Gardner, E. Berg, M. J. Manfra, A. Stern, C. M. Marcus, and F. Nichele, Evidence of topological superconductivity in planar Josephson junctions, Nature (London) **569**, 89 (2019).
[18] H. Ren, F. Pientka, S. Hart, A. T. Pierce, M. Kosowsky, L. Lunczer, R. Schlereth, B. Scharf, E. M. Hankiewicz, L. W. Molenkamp, B. I. Halperin, and A. Yacoby, Topological superconductivity in a phase-controlled Josephson junction, Nature (London) **569**, 93 (2019).
[19] F. Setiawan, A. Stern, and E. Berg, Topological superconductivity in planar Josephson junctions: Narrowing down to the nanowire limit, Phys. Rev. B **99**, 220506(R) (2019).
[20] J.-P. Xu, M.-X. Wang, Z. L. Liu, J.-F. Ge, X. Yang, C. Liu, Z. A. Xu, D. Guan, C. L. Gao, D. Qian, Y. Liu, Q.-H. Wang, F.-C. Zhang, Q.-K. Xue, and J.-F. Jia, Experimental Detection of a Majorana Mode in the core of a Magnetic Vortex inside a Topological Insulator-Superconductor $Bi_2Te_3/NbSe_2$ Heterostructure, Phys. Rev. Lett. **114**, 017001 (2015).
[21] H.-H. Sun, K.-W. Zhang, L.-H. Hu, C. Li, G.-Y. Wang, H.-Y. Ma, Z.-A. Xu, C.-L. Gao, D.-D. Guan, Y.-Y. Li, C. Liu, D. Qian, Y. Zhou, L. Fu, S.-C. Li, F.-C. Zhang, and J.-F. Jia, Majorana Zero Mode Detected with Spin Selective Andreev Reflection in the Vortex of a Topological Superconductor, Phys. Rev. Lett. **116**, 257003 (2016).
[22] J. Wiedenmann, E. Bocquillon, R. S. Deacon, S. Hartinger, O. Herrmann, T. M. Klapwijk, L. Maier, C. Ames, C. Brune, C. Gould, A. Oiwa, K. Ishibashi, S. Tarucha, H. Buhmann, and L. W. Molenkamp, 4π-periodic Josephson supercurrent in HgTe-based topological Josephson junctions, Nat. Commun. **7**, 10303 (2016).
[23] E. Bocquillon, R. S. Deacon, J. Wiedenmann, P. Leubner, T. M. Klapwijk, C. Brune, K. Ishibashi, H. Buhmann, and L. W. Molenkamp, Gapless Andreev bound states in the quantum spin Hall insulator HgTe, Nat. Nanotechnol. **12**, 137 (2017).
[24] C. Li, J. C. de Boer, B. de Ronde, S. V. Ramankutty, E. van Heumen, Y. Huang, A. de Visser, A. A. Golubov, M. S. Golden, and A. Brinkman, 4π-periodic Andreev bound states in a Dirac semimetal, Nat. Mater. **17**, 875 (2018).
[25] A.-Q. Wang, C.-Z. Li, C. Li, Z.-M. Liao, A. Brinkman, and D.-P. Yu, 4π Periodic Supercurrent from Surface States in Cd_3As_2 Nanowire-Based Josephson Junctions, Phys. Rev. Lett. **121**, 237701 (2018).
[26] W. Yu, W. Pan, D. L. Medlin, M. A. Rodriguez, S. R. Lee, Z.-q. Bao, and F. Zhang, π and 4π Josephson Effects Mediated by a Dirac Semimetal, Phys. Rev. Lett. **120**, 177704 (2018).
[27] Z. Lyu, Y. Pang, J. Wang, G. Yang, J. Fan, G. Liu, Z. Ji, X. Jing, C. Yang, F. Qu, and L. Lu, Protected gap closing in Josephson junctions constructed on Bi_2Te_3 surface, Phys. Rev. B **98**, 155403 (2018).
[28] G. Yang, Z. Lyu, J. Wang, J. Ying, X. Zhang, J. Shen, G. Liu, J. Fan, Z. Ji, X. Jing, F. Qu, and L. Lu, Protected gap closing in Josephson trijunctions constructed on Bi_2Te_3, Phys. Rev. B **100**, 180501(R) (2019).
[29] S. Cho, B. Dellabetta, R. Zhong, J. Schneeloch, T. Liu, G. Gu, M. J. Gilbert, and N. Mason, Aharonov–Bohm oscillations in a quasi-ballistic three-dimensional topological insulator nanowire, Nat. Commun. **6**, 7634 (2015).
[30] L. A. Jauregui, M. T. Pettes, L. P. Rokhinson, L. Shi, and Y. P. Chen, Magnetic field-induced helical mode and topological transitions in a topological insulator nanoribbon, Nat. Nanotechnol. **11**, 345 (2016).
[31] H. Pan, M. Wu, Y. Liu, and S. A. Yang, Electric control of topological phase transitions in Dirac semimetal thin films, Sci. Rep. **5**, 14639 (2015).
[32] J. L. Collins, A. Tadich, W. Wu, L. C. Gomes, J. N. B. Rodrigues, C. Liu, J. Hellerstedt, H. Ryu, S. Tang, S.-K. Mo, S. Adam, S. A. Yang, M. S. Fuhrer, and M. T. Edmonds, Electric-field-tuned topological phase transition in ultrathin Na_3Bi, Nature (London) **564**, 390 (2018).
[33] J. Liu, T. H. Hsieh, P. Wei, W. Duan, J. Moodera, and L. Fu, Spin-filtered edge states with an electrically tunable gap in a two-dimensional topological crystalline insulator, Nat. Mater. **13**, 178 (2014).
[34] D. Shao, J. Ruan, J. Wu, T. Chen, Z. Guo, H. Zhang, J. Sun, L. Sheng, and D. Xing, Strain-induced quantum topological phase transitions in Na_3Bi, Phys. Rev. B **96**, 075112 (2017).
[35] T. Nie, L. Meng, Y. Li, Y. Luan, and J. Yu, Phase transition studies of Na_3Bi system under uniaxial strain, J. Phys. Condens. Matter **30**, 125502 (2018).
[36] H. Wang, H. Wang, H. Liu, H. Lu, W. Yang, S. Jia, X.-J. Liu, X. C. Xie, J. Wei, and J. Wang, Observation of superconductivity induced by a point contact on 3D Dirac semimetal Cd_3As_2 crystals, Nat. Mater. **15**, 38 (2016).
[37] L. Aggarwal, A. Gaurav, G. S. Thakur, Z. Haque, A. K. Ganguli, and G. Sheet, Unconventional superconductivity at mesoscopic point contacts on the 3D Dirac semimetal Cd_3As_2, Nat. Mater. **15**, 32 (2016).
[38] L. He, Y. Jia, S. Zhang, X. Hong, C. Jin, and S. Li, Pressure-induced superconductivity in the three-dimensional topological Dirac semimetal Cd_3As_2, npj Quantum Mater. **1**, 16014 (2016).
[39] C.-Z. Li, L.-X. Wang, H. Liu, J. Wang, Z.-M. Liao, and D.-P. Yu, Giant negative magnetoresistance induced by the chiral anomaly in individual Cd_3As_2 nanowires, Nat. Commun. **6**, 10137 (2015).
[40] See Supplemental Material at http://link.aps.org/supplemental/10.1103/PhysRevLett.126.027001 for sample growth and transport measurements, details of supercurrent interference, finite momentum shift due to Zeeman effect, and results of device 2, which includes Refs. [41–42].
[41] D. Son and B. Spivak, Chiral anomaly and classical negative magnetoresistance of Weyl metals, Phys. Rev. B **88**, 104412 (2013).
[42] C.-Z. Li, A.-Q. Wang, C. Li, W.-Z. Zheng, A. Brinkman, D.-P. Yu, and Z.-M. Liao, Reducing Electronic Transport Dimension to Topological Hinge States by Increasing Geometry Size of Dirac Semimetal Josephson Junctions, Phys. Rev. Lett. **124**, 156601 (2020).
[43] M. Neupane, S. Y. Xu, R. Sankar, N. Alidoust, G. Bian, C. Liu, I. Belopolski, T. R. Chang, H. T. Jeng, H. Lin, A. Bansil, F. Chou, and M. Z. Hasan, Observation of a three-

dimensional topological Dirac semimetal phase in high-mobility Cd_3As_2, Nat. Commun. **5**, 3786 (2014).

[44] S. Jeon, B. B. Zhou, A. Gyenis, B. E. Feldman, I. Kimchi, A. C. Potter, Q. D. Gibson, R. J. Cava, A. Vishwanath, and A. Yazdani, Landau quantization and quasiparticle interference in the three-dimensional Dirac semimetal Cd_3As_2, Nat. Mater. **13**, 851 (2014).

[45] Enze Zhang, Yanwen Liu, Weiyi Wang, Cheng Zhang, Peng Zhou, Z.-G. Chen, J. Zou, and F. Xiu, Magnetotransport properties of Cd_3As_2 nanostructures, ACS Nano **9**, 8843 (2015).

[46] L.-X. Wang, C.-Z. Li, D.-P. Yu, and Z.-M. Liao, Aharonov-Bohm oscillations in Dirac semimetal Cd_3As_2 nanowires, Nat. Commun. **7**, 10769 (2016).

[47] B.-C. Lin, S. Wang, L.-X. Wang, C.-Z. Li, J.-G. Li, D. Yu, and Z.-M. Liao, Gate-tuned Aharonov-Bohm interference of surface states in a quasiballistic Dirac semimetal nanowire, Phys. Rev. B **95**, 235436 (2017).

[48] C.-Z. Li, C. Li, L.-X. Wang, S. Wang, Z.-M. Liao, A. Brinkman, and D.-P. Yu, Bulk and surface states carried supercurrent in ballistic Nb-Dirac semimetal Cd_3As_2 nanowire-Nb junctions, Phys. Rev. B **97**, 115446 (2018).

[49] K. Flensberg, J. B. Hansen, and M. Octavio, Subharmonic energy-gap structure in superconducting weak links, Phys. Rev. B **38**, 8707 (1988).

[50] C.-Z. Li, A.-Q. Wang, C. Li, W.-Z. Zheng, A. Brinkman, D.-P. Yu, and Z.-M. Liao, Fermi-arc supercurrent oscillations in Dirac semimetal Josephson junctions, Nat. Commun. **11**, 1150 (2020).

[51] K. Gharavi, G. W. Holloway, C. M. Haapamaki, M. H. Ansari, M. Muhammad, R. R. LaPierre, and J. Baugh, Josephson interference due to orbital states in a nanowire proximity effect junction, arXiv:1405.7455.

[52] K. Gharavi and J. Baugh, Orbital Josephson interference in a nanowire proximity-effect junction, Phys. Rev. B **91**, 245436 (2015).

[53] K. Zuo, V. Mourik, D. B. Szombati, B. Nijholt, D. J. van Woerkom, A. Geresdi, J. Chen, V. P. Ostroukh, A. R. Akhmerov, S. R. Plissard, D. Car, E. P. A. M. Bakkers, D. I. Pikulin, L. P. Kouwenhoven, and S. M. Frolov, Supercurrent Interference in Few-Mode Nanowire Josephson Junctions, Phys. Rev. Lett. **119**, 187704 (2017).

[54] B.-C. Lin, S. Wang, A.-Q. Wang, Y. Li, R.-R. Li, K. Xia, D. Yu, and Z.-M. Liao, Electric Control of Fermi Arc Spin Transport in Individual Topological Semimetal Nanowires, Phys. Rev. Lett. **124**, 116802 (2020).